CrossMark

ORIGINAL ARTICLE

Effects of aging on T_1, T_2^*, and QSM MRI values in the subcortex

M. C. Keuken[1,2] · P.-L. Bazin[3] · K. Backhouse[1] · S. Beekhuizen[1] · L. Himmer[1] ·
A. Kandola[1] · J. J. Lafeber[1] · L. Prochazkova[1] · A. Trutti[1] · A. Schäfer[4] · R. Turner[1,3] ·
B. U. Forstmann[1,2]

Abstract The aging brain undergoes several anatomical changes that can be measured with Magnetic Resonance Imaging (MRI). Early studies using lower field strengths have assessed changes in tissue properties mainly qualitatively, using T_1- or T_2^*- weighted images to provide image contrast. With the development of higher field strengths (7 T and above) and more advanced MRI contrasts, quantitative measures can be acquired even of small subcortical structures. This study investigates volumetric, spatial, and quantitative MRI parameter changes associated with healthy aging in a range of subcortical nuclei, including the basal ganglia, red nucleus, and the periaqueductal grey. The results show that aging has a heterogenous effects across regions. Across the subcortical areas an increase of T_1 values is observed, most likely indicating a loss of myelin. Only for a number of areas, a decrease of T_2^* and increase of QSM is found, indicating an increase of iron. Aging also results in a location shift for a number of structures indicating the need for visualization of the anatomy of individual brains.

Keywords Ultra-high field 7 T MRI · T_1 · T_2^* · QSM · Subcortex · Basal ganglia · Aging

Introduction

Healthy aging across the adult lifespan is known to have a diverse effect on the anatomy of the brain. Historically, anatomical studies were performed on post-mortem specimens but with the development of magnetic resonance imaging (MRI) in vivo individual anatomy can now be visualized non-invasively. Several age-related findings which are frequently reported are the ventricular enlargement (e.g., Good et al. 2001; Raz and Rodrigue 2006; Greenberg et al. 2008; Keuken et al. 2013), changes in white matter microstructure (e.g., Walhovd et al. 2005; Benedetti et al. 2006; Raz and Rodrigue 2006), reduced grey matter volume (e.g., Courchesne et al. 2000; Good et al. 2001; Cherubini et al. 2009; Lemaitre et al. 2012), shifted location of gray matter nuclei (e.g., Dunnen and Staal 2005; Kitajima et al. 2008; Keuken et al. 2013; Mavridis et al. 2014), and an increase in iron deposition (e.g., Hallgren and Sourander 1958; Schenker et al. 1993; Zecca et al. 2004; Raz and Rodrigue 2006; Aquino et al. 2009; Pfefferbaum et al. 2009). These aging effects can vary locally across the brain (e.g., Greenberg et al. 2008; Cherubini et al. 2009; Draganski et al. 2011; Lemaitre et al. 2012). In addition to these anatomical changes, previous work shows changes in MRI parameters with age (e.g., Schenker et al. 1993; Steen et al. 1995; Courchesne et al. 2000; Good et al. 2001; Benedetti et al. 2006; Bastin et al. 2009; Saito et al. 2009; Cherubini et al. 2009; Draganski et al. 2011; Bilgic et al. 2012; Lebel et al. 2012; Lemaitre et al. 2012; Li et al. 2013; Yeatman et al. 2014; Lorio et al. 2014; Persson et al. 2015; Acosta-Cabronero et al. 2016; Betts et al. 2016). Changes in T_1 values are frequently reported and have been interpreted as

✉ M. C. Keuken
  mckeuken@gmail.com

[1] Integrative Model-based Cognitive Neuroscience Research Unit, University of Amsterdam, Amsterdam, The Netherlands

[2] Netherlands Institute for Neuroscience, an Institute of the Royal Netherlands Academy of Arts and Sciences, Amsterdam, The Netherlands

[3] Max Planck Institute for Human Cognitive and Brain Sciences, Leipzig, Germany

[4] Siemens Healthcare GmbH, Diagnostic Imaging, Magnetic Resonance, Research and Development, Erlangen, Germany

changes in myelin structure (e.g., Silver et al. 1997; Maniega et al. 2015). Another common finding is the shortening of T_2^* values, which have been interpreted as an indication of iron accumulation (Daugherty and Raz 2013).

The T_1 value indicates the recovery time of the longitudinal component of the magnetization following the application of a radio frequency excitation pulse. The quantitative T_1 values correlate highly with myelin content (Koenig 1991; Stüber et al. 2014) and can be used as an in vivo proxy for the underlying myeloarchitecture (Lutti et al. 2014; Dinse et al. 2015). The T_2^* value indicates the decay of the transverse magnetization component as a result of proton interactions and magnetic field inhomogeneity. The T_2^* values have been used as a proxy for iron, but recently several studies have demonstrated that the T_2^* values are also strongly influenced by the presence and orientation of myelin (Fukunaga et al. 2010; Lee et al. 2010; Cohen-Adad et al. 2012; Stüber et al. 2014). Iron content in gray matter can be estimated more precisely using a post-processing technique called Quantitative Susceptibility Mapping (QSM) on the phase signal present in the T_2^*-weighted volumes (Schweser et al. 2011, 2016; Bilgic et al. 2012; Langkammer et al. 2012; Stüber et al. 2014; Ropele and Langkammer 2016). QSM quantifies the susceptibility distribution by estimating the magnetic field distribution, removing the background field contribution, and solves the inverse problem from field perturbation to magnetic susceptibility (Schweser et al. 2016).

Many age-related MRI studies have been limited by the use of low field strength or qualitative MRI sequences. Using low field strength such as 1.5 or 3T makes it difficult to visualize smaller nuclei such as the subthalamic nucleus or to discriminate the internal and external segment of the globus pallidus (e.g., Cho et al. 2008, 2010; Abosch et al. 2010; Beisteiner et al. 2011; Lenglet et al. 2012; Keuken et al. 2014).

The current study set out to describe the effects of aging on the volumetric and spatial properties, and to provide quantitative T_1, T_2^*, and QSM values at 7T static magnetic field for the striatum (STR), external segment of the globus pallidus (GPe), the internal segment of the globus pallidus (GPi), the red nucleus (RN), the subthalamic nucleus (STN), the substantia nigra (SN), and the periaqueductal grey (PAG). This was done by manually parcellating the different regions in structural ultra-high resolution 7T MRI data in three different age groups.

Methods

Participants

Thirty young participants with an average age of 23.8 years (age range 19–29; SD = 2.3, 14 females) which have been

previously reported (Keuken et al. 2014) were included. In addition to the young participants, a second group of 14 middle-aged participants were scanned, with an average age of 52.5 years (age range 40–60, SD = 6.6, 7 females). Finally, a third group of 10 elderly participants were included, with an average age of 69.6 years (age range 60–75, SD = 4.6, 3 females). One elderly subject (male, age 73) did not complete all scans due to time constraints and was excluded from all further analyses. All subjects were right-handed, as confirmed by the Edinburgh Inventory (Oldfield 1971). None of the participants had a history of neurological disorders or currently suffered from psychiatric disorders as indicated by self-report and structured clinical interview. The study was approved by the local ethical committee of the Max Planck Institute for Human Brian and Cognitive Sciences in Leipzig, Germany.

MRI acquisition

The structural data were acquired using a 7T Siemens Magnetom MRI scanner using a 24-channel head array Nova coil (NOVA Medical Inc., Wilmington MA) and consisted of three sequences: a whole brain MP2RAGE (Marques et al. 2010), a MP2RAGE covering a smaller slab, and a multi-echo 3D FLASH (Haase et al. 1986). The whole brain MP2RAGE had 240 sagittal slices with an acquisition time of 10:57 min (repetition time (TR) = 5000 ms; echo time (TE) = 2.45 ms; inversion times TI1/TI2 = 900/2750 ms; flip angle = 5°/3°; bandwidth = 250 Hz/Px; voxel size = 0.7 mm isotropic). The MP2RAGE slab consisted of 128 slices with an acquisition time of 9:07 min (TR = 5,000 ms; TE = 3.71 ms; TI1/TI2 = 900/2,750 ms; flip angle = 5°/3°; bandwidth = 240 Hz/Px; voxel size = 0.6 mm isotropic). The MP2RAGE sequence is a T_1-weighted structural scan but with the additional feature that it also provides a so-called T_1 map (Marques et al. 2010). The sequence is based on two volumes with different inversion times (the INV1 and INV2 volumes), which can be combined into a single T_1-weighted volume (UNI) or used to estimate the T_1 values. The resulting T_1 map gives reasonable estimates of the underlying T_1 values and has been shown to be highly reliable within subjects across scan sessions and scanners (Okubo et al. 2015; Voelker et al. 2016). It should, however, be noted that these T_1 maps may still contain residual transmit field bias (Marques and Gruetter 2013; Lutti et al. 2014).

The FLASH slab consisted of 128 slices with an acquisition time of 17:18 min (TR = 41 ms and three different TE: 11.22/20.39/29.57 ms; flip angle = 14°; bandwidth = 160 Hz/Px; voxel size = 0.5 mm isotropic). Both slab sequences consisted of axial slices tilted −23° to the true axial plane in scanner coordinates. See (Forstmann et al. 2014) for more information regarding the exact MRI

parameters and data quality. All structural data have been made freely available and can be found on http://www. nitrc.org/projects/atag_mri_scans/ and http://datadryad.org/ resource/doi:10.5061/dryad.fb41s.

Manual parcellation of subcortical structures

The STR, GPe, GPi, RN, STN, and SN masks for the young group have been previously presented in (Keuken et al. 2014). For the young group, the PAG, lateral ventricle, third ventricle, cerebral aqueduct, and fourth ventricle were additionally parcellated and have not been published previously in the young group for this study. For the middle-aged and elderly group the STR, GPe, GPi, RN, STN, SN, PAG, lateral ventricle, third ventricle, cerebral aqueduct, and fourth ventricle were parcellated using the same parcellation protocol (Keuken et al. 2014). In short, the manual parcellation was performed using the FSL 4.1.4 viewer (http://fsl.fmrib.ox.ac.uk/fsl/fslview/) by two independent raters. Based on previous results (Keuken et al. 2014) the STR was segmented on the UNI MP2RAGE slab volumes, the STN, SN, and RN on the FLASH volumes, and finally the GPe and GPi on the QSM volumes. The PAG and ventricle system were parcellated on the UNI MP2RAGE whole brain volumes. The resolution and lack of contrast of the in vivo MP2RAGE scans made it very difficult to distinguish the different sub compartments of the STR (Voorn et al. 2004; Haber and Gdowski 2004; Neto et al. 2008; Haber and Knutson 2009; Keuken et al. 2014). Therefore, the STR was segmented as a whole without attempting to make distinctions between the different subparts which would have to be based on surrounding landmarks. The GPe and GPi were segmented on the QSM images as the T_2^* image quality was not sufficient to clearly separate the interlamina between the GPe and GPi, whereas this was the case for the QSM (Keuken et al. 2014).

After parcellation of the structure, the inter-rater agreement was assessed using the Dice coefficient (Dice 1945). The resulting conjunction masks were used for further analysis unless stated otherwise. All volume estimates are calculated in the native space of the MRI sequence in which the structure was parcellated. The intracranial volume estimate was calculated using the skull stripped whole brain MP2RAGE unified volume, using BET (Smith 2002). Because the whole brain MP2RAGE scan was skull stripped automatically, no inter-rater agreement was assessed.

Due to the time-consuming nature of manual parcellation, it was not possible to have the same raters for the middle-aged and elderly group as in the young group that was published previously (Keuken et al. 2014). Therefore, it might be the case that some of the effects of aging are actually due to different raters for the young age group versus the middle-aged and elderly group. To test whether this could influence the general conclusion, the same raters that segmented the RN and STN for the middle-aged and elderly group, redid the parcellation for the young RN and STN masks, which allowed testing the influence on the results of different raters for different age groups.

Registration to standard stereotactic MNI-space

The third echo time of the FLASH sequence was linearly registered to the MP2RAGE slab second inversion volume using Mutual information and 6 Degrees of Freedom (DoF). The MP2RAGE slab second inversion volume was registered to the MP2RAGE whole brain second inversion volume using correlation ratio information and 6 DoF. The MP2RAGE whole brain unified volumes were registered to the MNI152 0.5 mm template using correlation ratio information and 12 DoF. All linear registrations used trilinear interpolation and were done using FLIRT (Jenkinson and Smith 2001; Jenkinson et al. 2002) as implemented in FSL 5.0.2. Prior to the registration to MNI standard space, both the MP2RAGE whole brain and MNI152 template were skull stripped using BET (Smith 2002). Finally, the MP2RAGE whole brain unified volumes were non-linearly registered to the MNI152 0.5 mm template using the linearly registered volumes as input for FNIRT in combination with the default settings of FNIRT (Andersson et al. 2007; Jenkinson et al. 2012). The FLASH and MP2RAGE slab images were transformed to the MNI152 template by combining the resulting transformation matrices from the FLASH to MP2RAGE slab, MP2RAGE slab to MP2RAGE whole brain, and MP2RAGE whole brain to MNI152 registration. All individual registration steps were visually checked for misalignment. All parcellated structures were transformed to the MNI152 template using the corresponding transformation matrices and added together to create a probabilistic atlas of each structure separately. This was done both for the linear and non-linearly registered structures. All the probabilistic atlases are made freely available and can be found on https://www.nitric.org/projects/atag/. See Fig. 1 for a flowchart of the registration pipeline.

Statistical analyses were done in R 3.2.4 (http://www.r-project.org; R Development Core Team 2013). All correlation and partial correlation tests were done using a two-sided Pearson's r test with a critical α of 0.05 using the individual age as a continuous variable. The three age groups were only used as a discrete variable to provide the summary statistics. A Bonferroni correction was used to correct for multiple comparisons per family of tests. For instance, the Bonferroni correction for the correlations between age and the Dice coefficient was based on 11 tests which correspond to the number of structures for which the Dice coefficient was calculated. All reported p values are
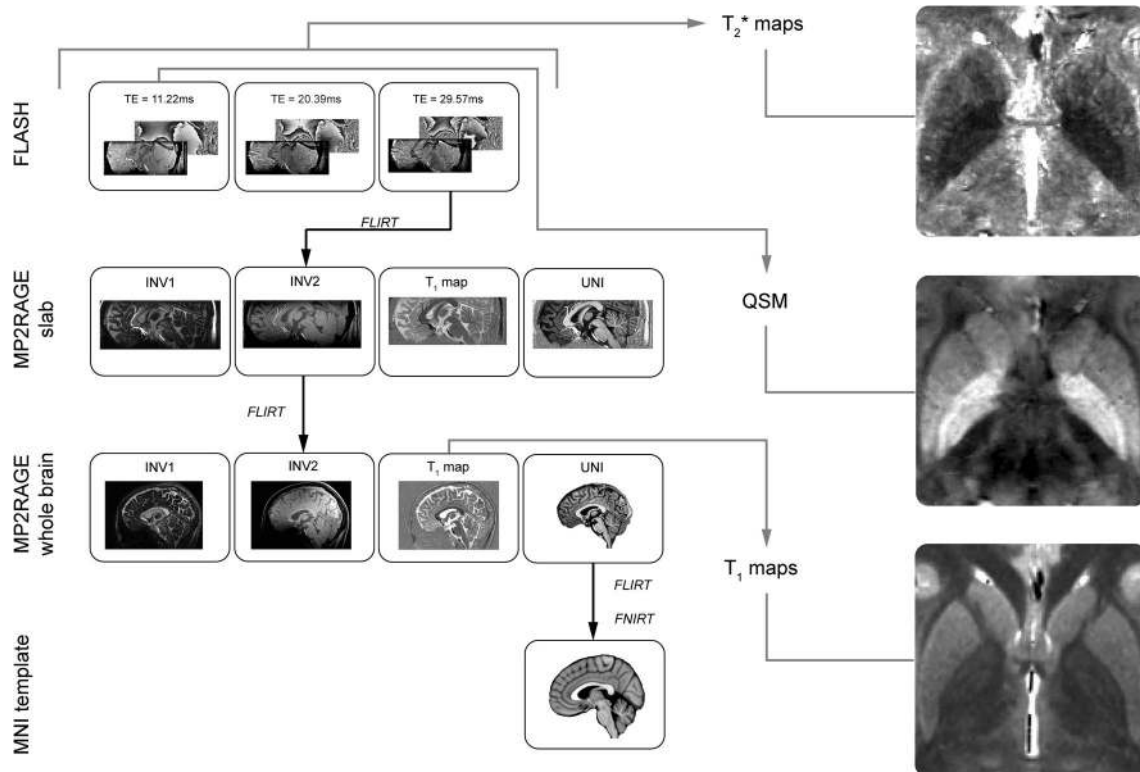
Fig. 1 The registration pipeline. The RN, STN, and SN were parcellated on the FLASH volumes. The GPe and GPi were parcellated on the QSM volumes which were based on the first echo time of the FLASH volumes. The STR was parcellated on the MP2RAGE slab UNI volume whereas the ventricle compartments and the PAG were parcellated on the MP2RAGE whole brain UNI volume. Using the resulting transformation matrices, the conjunction masks were transformed to the T_2^*, QSM, or T_1 map space so that the quantitative MRI values could be extracted. Examples of the T_2^*, QSM, and T_1 maps of a young participant are shown on the *right*

after Bonferroni correction. For all significant correlations, 95% confidence intervals were estimated using the function *predict* as implemented in R and plotted in Figs. 2 and 3

Effect of age on location

To test whether age had an effect on the location of the gray matter nuclei in standard MNI space, the following analysis was done. First, the Center of Mass (CoM) was calculated for each linear registered structure using FSLUTILS (FSL 5.0.2). To reduce the number of tests, a Principal Component Analysis (PCA) was computed on the X, Y, and Z CoM coordinates of each individual structure using *princomp* in R Team (2013). Since we had no a-priori hypothesis regarding lateralization and age, the negative X-coordinate values, corresponding to the left hemisphere, were converted to positive values and combined in a single PCA analysis. The resulting first principal component corresponds to a new latent variable which captures the maximal amount of variance. Finally, the eigenvector scores of the first principal component of each structure and participant were correlated with age. This analysis allows us to test whether there is a relationship between the individual

spatial location, as indicated by the individual eigenvector scores, and age.

Computation of the T_1, T_2^*, and QSM values

The T_1 values for the STR, GPe, GPi, RN, STN, SN, and PAG were extracted from the MP2RAGE whole brain T_1 map. The T_2^* values for the STR, GPe, GPi, RN, STN, SN, and PAG were calculated using the T_2^* fitting module as implemented in the CBS High-Res Brain Processing Tools for MIPAV (http://www.nitrc.org/projects/cbs-tools/) (Bazin et al. 2013). This module uses a nonlinear least squares function to estimate a single-component T_2^* map (Whittall et al. 1997):

$$S(\text{TE}) = S_0 e^{(-\text{TE}/T_2^*)}.$$

Possibly due to the interpolation between different MRI scans or intrinsic partial voluming, the STR and PAG masks contained voxels which, based on the T_1, T_2^* values, and the spatial location, belonged to the lateral ventricle or cerebral aqueduct. Extracting the mean T_1 and T_2^* values from these voxels would result in a skewed estimate given that the T_1 and T_2^* values of the CSF are considerably
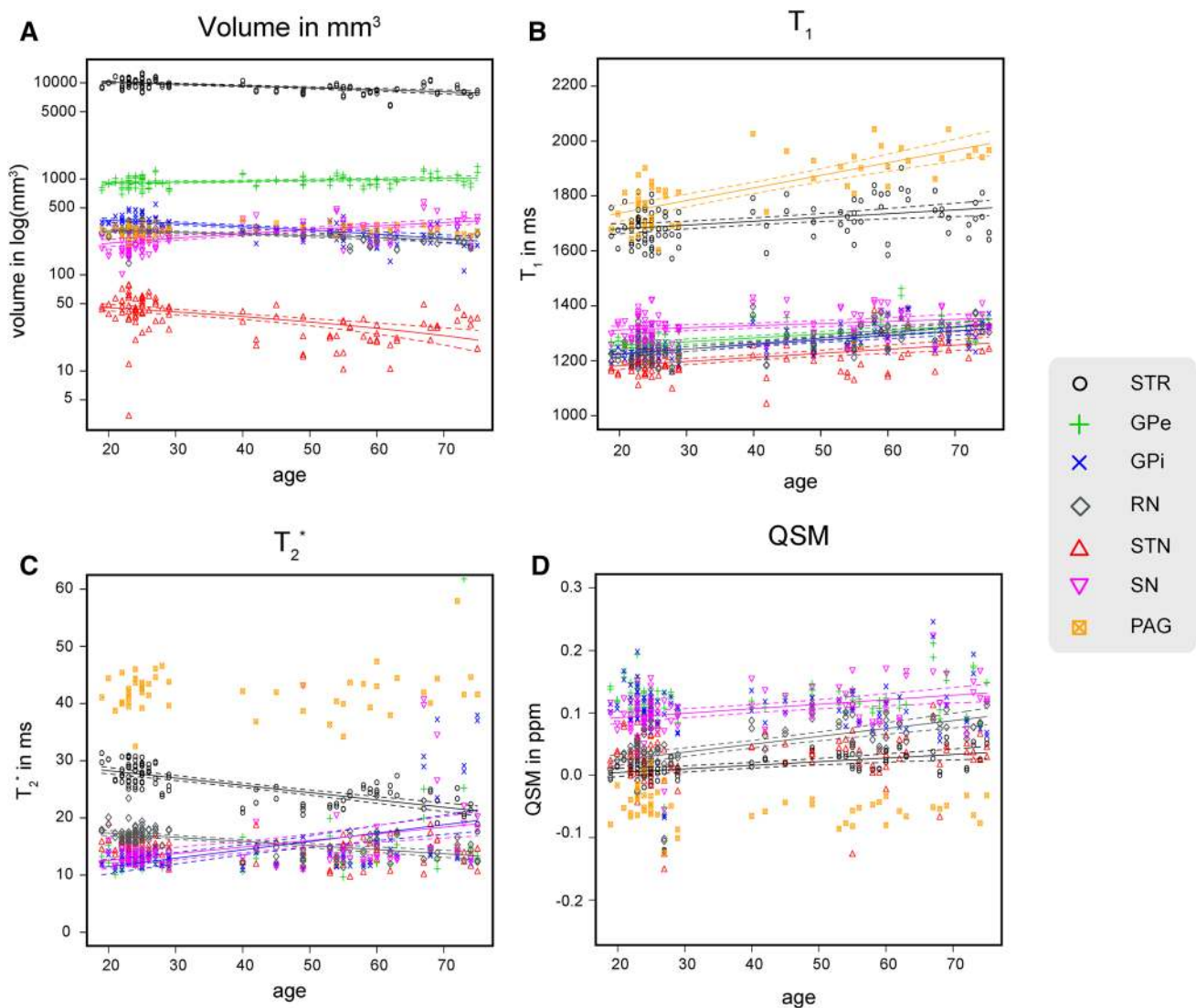
Fig. 2 The volume, T_1, T_2^*, and QSM values per structure for each individual participant. The regression lines indicate a significant correlation with age. The *dotted lines* indicate the 95% confidence interval. *STR* striatum, *GPe* globus pallidus externa, *GPi* globus pallidus interna, *RN* red nucleus, *STN* subthalamic nucleus, *SN* substantia nigra, *PAG* periaqueductal *grey*

distinct from those in the gray matter ROIs (McRobbie et al. 2006). We addressed this by calculating the mean T_1 and T_2^* values of the ventricle compartment or the cerebral aqueduct and used that value as an upper threshold when extracting the mean T_1 and T_2^* values for the STR and PAG. For completeness we also tested the effects of aging on the non-thresholded T_1 and T_2^* values for the STR and PAG.

The QSM was calculated using the phase information of the first echo time of the FLASH acquisition and the method proposed by Schweser et al. (2012). The first echo time was chosen because it had the highest absolute SNR. The coil combination of phase data was done automatically by the scanner vendor software (version VB17). This automatic coil combination results in some minor phase singularities, but are partially accounted by

the employed superfast dipole inversion (SDI) approach which, includes a modified SHARP algorithm. The modified SHARP algorithm is described in Schweser et al. (2012). The masking of the data was done using BET which was manually adjusted if the binary mask was too lenient. This was determined by visual inspection on a subject to subject basis. The QSM intensities were normalized by subtracting the mean QSM value of the combined lateral ventricle conjunction masks from the main QSM volume. This normalisation was necessary due to the arbitrary settings of the resonance frequency, use of high pass filtering, and the use of a single echo to calculate the QSM values (Schäfer et al. 2009; Langkammer et al. 2012). To ensure that no gray matter tissue was included in the lateral ventricle masks, the masks were
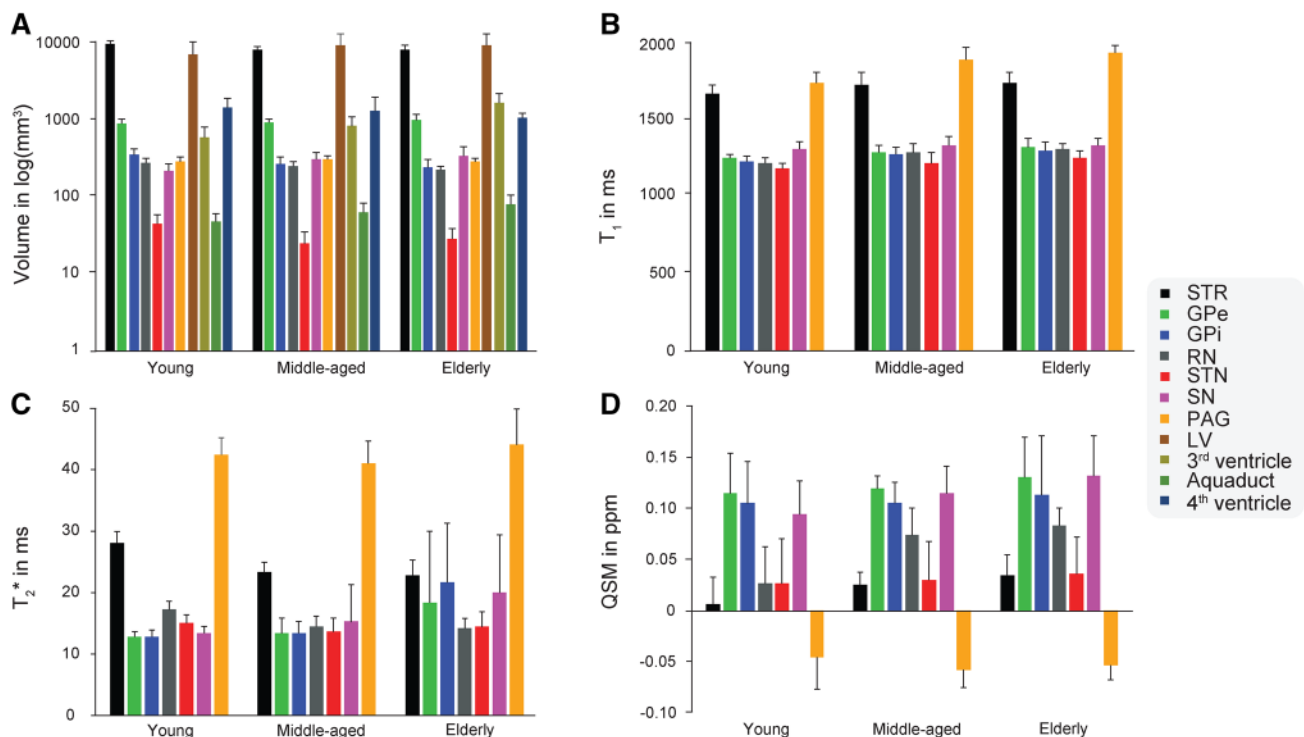
Fig. 3 The average volume, T_1, T_2^*, and QSM values across hemispheres per structure for each age group. The error bars indicate 1 sd. *STR* striatum, *GPe* globus pallidus externa, *GPi* globus pallidus interna, *RN* red nucleus, *STN* subthalamic nucleus, *SN* substantia nigra, *PAG* periaqueductal grey, *LV* lateral ventricle

first eroded with a 2 mm Gaussian kernel. All T_1-, T_2^*-maps, and QSM were calculated in native space.

Results

Inter-rater reliability

All segmentations resulted in a good to excellent mean agreement between the two raters, indicating that it is feasible to identify these subcortical structures in individual space. See Table 1 for the Dice coefficient per structure and age group. There were, however, different effects of age on the inter-rater reliability for these separate structures. For the STR, RN, SN, LV, and third ventricle there were positive correlations between the Dice coefficient and age (STR: $r = 0.58$, t(104) = 7.22, $p < 0.001$; RN: $r = 0.48$, t(104) = 5.57, $p \leq 0.001$; SN: $r = 0.33$, t(104) = 3.59, $p = 0.006$; third ventricle: $r = 0.63$, t(51) = 5.75, $p < 0.001$), indicating that the inter-rater reliability increases with age. This was the opposite for the GPe and the GPi as there was a negative correlation between the Dice coefficient and age (GPe: $r = -0.46$, t(104) = −5.30, $p < 0.001$; GPi: $r = -0.54$, t(104) = −6.62, $p < 0.001$). There was no significant correlation between the Dice coefficient and age for the STN, PAG, LV, cerebral aqueduct, and fourth ventricle.

The variability in inter-rater reliability between the structures and age ranges could be considered a confounding factor for any further analysis. We addressed this by incorporating the Dice coefficient as a covariate in all further analyses unless stated otherwise.

Effect of different raters

The correlation between the Dice coefficient and age for the STN and RN did not statistically change whether the previously published masks were used or the new parcellation (RN: $r = 0.45$, t(104) = 5.18, $p < 0.001$ versus $r = 0.48$, t(104) = 5.57, $p < 0.001$; STN: $r = -0.18$, t(104) = −1.99, $p = 0.062$ versus $r = 0.07$, t(104) = 0.75, $p = 0.46$ respectively). As indicated by the Fisher r-to-z transformation (Steiger 1980), the correlations did not statistically differ (RN: $Z = -0.27$, $p = 0.79$; STN: $Z = -1.81$, $p = 0.07$). The volumetric effects of age for the RN and the STN were also independent of which masks were used for the young group (RN: $r = -0.55$, t(106) = −6.73, $p < 0.001$ versus $r = -0.53$, t(106) = −6.26, $p < 0.001$; STN: $r = -0.70$, t(106) = −9.89, $p < 0.001$ versus $r = -0.67$, t(106) = −9.11, $p < 0.001$, respectively). As indicated by the Fisher r-to-z transformation, the correlations did not statistically differ (RN: $Z = -0.2$, $p = 0.84$; STN: $Z = -0.41$ $p = 0.68$).

2493

Table 1 The inter-rater reliability coefficient and conjunction volume in mm³ estimates

Structure	Young Volume Mean mm³	SD	Young Dice Mean	SD	Middle aged Volume Mean mm³	SD	Middle Dice Mean	SD	Elderly Volume Mean mm³	SD	Elderly Dice Mean	SD
Intracranial volume	1545970.0	113255.60	–	–	1523494.0	117079.20	–	–	1546127.0	172959300.0	–	–
STR												
Left	10128.62‡	1038.96	0.89	0.01	8586.88	903.45	0.9	0.01	8466.28	1334.86	0.91	0.01
Right	10064.2‡	1051.34	0.89	0.01	8423.03	723.4	0.89	0.01	8370.9	1506.64	0.91	0.01
Overall	10096.41‡	1036.78	0.89	0.01	8504.95	807.42	0.9	0.01	8418.59	1381.72	0.91	0.01
GPe												
Left	932.47‡	124.16	0.87	0.02	972.34	115.55	0.83	0.08	1056.35	181.07	0.85	0.02
Right	904.5‡	123.09	0.88	0.01	963.31	108.36	0.86	0.03	1007.08	143.92	0.84	0.03
Overall	918.49‡	123.38	0.88	0.02	967.84	110.02	0.84	0.06	1033.59	160.87	0.84	0.02
GPi												
Left	366.63‡	63.16	0.82	0.03	267.98	53.31	0.77	0.07	244.82	47.06	0.74	0.08
Right	365.11‡	57.42	0.84	0.03	286.31	63.26	0.8	0.05	248.19	90.29	0.75	0.08
Overall	365.87‡	59.85	0.83	0.03	277.15	58.16	0.79	0.06	247.01	69.85	0.74	0.08
RN_1												
Left	285.05‡	49.42	0.89	0.03	–	–	–	–	–	–	–	–
Right	276.85‡	49.79	0.89	0.03	–	–	–	–	–	–	–	–
Overall	280.95	49.36	0.89	0.03	–	–	–	–	–	–	–	–
RN_2												
Left	290.76	40.39	0.88	0.03	260.69	35.21	0.92	0.02	239.07	33.38	0.91	0.02
Right	279.1	43.58	0.89	0.02	253.35	38.02	0.93	0.02	228.93	31.84	0.92	0.01
Overall	284.93	42.07	0.89	0.03	257.02	36.15	0.92	0.02	234.0	32.07	0.92	0.02
STN_1												
Left	52.83‡	16.26	0.72	0.14	–	–	–	–	–	–	–	–
Right	59.5‡	15.71	0.76	0.09	–	–	–	–	–	–	–	–
Overall	56.17‡	16.2	0.74	0.12	–	–	–	–	–	–	–	–
STN_2												
Left	40.75	12.05	0.66	0.14	25.46	9.07	0.72	0.07	29.71	8.95	0.71	0.09
Right	50.07	14.53	0.71	0.14	24.99	9.19	0.7	0.09	28.72	11.46	0.68	0.1
Overall	45.41	14.04	0.68	0.14	25.22	8.96	0.71	0.08	29.22	9.99	0.69	0.09
SN												
Left	223.18‡	46.79	0.76	0.05	319.55	73.21	0.79	0.04	369.72	114.84	0.79	0.07
Right	226.33‡	50.46	0.76	0.04	313.26	77.96	0.79	0.07	331.83	97.77	0.79	0.04
Overall	224.75‡	48.27	0.76	0.04	316.4	74.28	0.79	0.06	350.78	105.28	0.79	0.06
PAG	292.25	40.47	0.79	0.04	315.76	33.76	0.82	0.03	292.05	28.59	0.78	0.04

Table 1 (continued)

Structure	Young						Middle aged						Elderly					
	Volume			Dice coefficient			Volume			Dice coefficient			Volume			Dice coefficient		
	Mean mm³	SD		Mean	SD		Mean mm³	SD		Mean	SD		Mean mm³	SD		Mean	SD	
LV																		
Left	7829.75	3367.64		0.89	0.03		10001.19	3844.15		0.89	0.02		13728.48	3657.5		0.91	0.02	
Right	7220.83	3579.82		0.87	0.04		9579.08	3776.74		0.87	0.05		14322.18	5622.29		0.91	0.02	
Overall	7525.29	3459.43		0.88	0.04		9790.54	3745.54		0.88	0.04		14025.33	4611.28		0.91	0.02	
3rd	606.47	205.54		0.69	0.07		859.32	263.74		0.76	0.06		1756.09	536.94		0.82	0.03	
Aquaduct	49.52	12.43		0.72	0.06		63.72	20.95		0.73	0.05		82.55	25.47		0.76	0.05	
4th	1514.64	521.67		0.74	0.11		1356.6	641.71		0.75	0.07		1091.12	178.11		0.66	0.12	

Rater 1 was constant across structures and participants

STR striatum, *GPe* globus pallidus externa, *GPi* globus pallidus interna, *RN* red nucleus, *STN* subthalamic nucleus, *SN* substantia nigra, *PAG* periaqueductal grey, *LV* lateral ventricle, *3rd* third ventricle, *Aqueduct* cerebral aqueduct, *4th* fourth ventricle. *_1* rater pair between rater 1 and rater 2; *_2* rater pair between rater 1 and rater 3

‡Previously published in Keuken et al. (2014)

These results indicate that the effect of rater pair is minimal compared to the effect of age since the Dice coefficient and volumetric results with age did not statistically change depending on the rater pair. All results that follow which include the RN and STN masks of the young participants are based on the rater pair who also parcellated the middle-aged and elderly participants.

Effect of aging on volume

In line with previous work (Courchesne et al. 2000; Ge et al. 2002; Mortamet et al. 2005), there was no significant effect of age on the intracranial volume. The STR, GPi, RN, and STN all showed a decrease in volume with age (STR: $r = -0.65$, t(106) $= -8.68$, $p < 0.001$; GPi: $r = -0.40$, t(106) $= -4.44$, $p < 0.001$; RN: $r = -0.53$, t(106) $= -6.26$, $p < 0.001$ STN: $r = -0.67$, t(106) $= -9.11$, $p < 0.001$). However, somewhat unexpectedly, both the GPe and SN showed a positive correlation between volume and age ($r = 0.33$, t(106) $= 3.535$, $p = 0.007$; $r = 0.53$, t(106) $= 6.33$, $p < 0.001$). While positive relations between grey matter volume and age have been previously reported in the literature (Mueller et al. 1998; Salat et al. 2002, 2004; Lemaitre et al. 2012) these are usually interpreted as an artefact of the employed method or measurement error. While we have no reason to assume that the employed MRI sequence and segmentation protocol were biased towards the GPe and SN, the volumetric results are counterintuitive and should be interpreted with caution. In line with previous work (Fjell and Walhovd 2010), the LV, third ventricle and the cerebral aqueduct showed a significant increase in volume with age (LV: $r = 0.54$, t(106) $= 6.51$, $p < 0.001$; third ventricle: $r = 0.45$, t(53) $= 3.56$, $p = 0.009$; cerebral aqueduct: $r = 0.52$, t(53) $= 4.36$, $p < 0.001$), whereas the PAG and the fourth ventricle did not show a significant increase in volume with age. Overall, the total volume of the parcellated ventricle compartments indicated an increase with age ($r = 0.47$, t(53) $= 3.81$, $p < 0.001$). See Fig. 2a for the volumetric results of the gray matter nuclei; Table 1 and Fig. 3a for the average values per age group.

Effect of aging on the location

To test whether aging had an effect on the spatial location of the different gray matter structures, the scores along the first eigenvector of the PCA analysis were correlated with the age of the participants while controlling for the Dice coefficient and the total ventricle volume. The total ventricle volume was included as a covariate since age and ventricle volume were strongly correlated, and ventricular expansion may affect the location of subcortical nuclei. In line with previous work there were several structures that showed a significant effect of age on the spatial location

Table 2 The mean and standard deviation of the T_1 values in ms per structure and age group

Structure	Young		Middle-aged		Elderly	
	Mean	SD	Mean	SD	Mean	SD
STR						
Left	1643.71	39.53	1703.71	71.78	1721.40	62.53
Right	1723.51	41.30	1762.79	70.91	1774.38	73.01
Overall	1683.61	56.79	1733.25	76.20	1747.01	71.35
GPe						
Left	1245.14	28.61	1287.44	48.81	1328.26	64.87
Right	1277.72	30.54	1304.99	45.35	1344.61	63.03
Overall	1261.43	33.62	1296.22	47.09	1336.44	62.61
GPi						
Left	1223.43	32.29	1279.28	48.88	1310.55	56.11
Right	1241.45	31.76	1284.55	41.49	1316.10	55.39
Overall	1232.44	33.03	1281.91	44.57	1313.33	54.16
RN						
Left	1235.49	38.80	1296.25	61.35	1319.50	30.74
Right	1225.58	34.18	1291.36	55.81	1315.22	30.16
Overall	1230.54	36.60	1293.80	57.60	1317.36	29.62
STN						
Left	1182.41	36.77	1215.14	74.46	1238.13	49.13
Right	1202.12	39.10	1228.43	74.75	1292.45	39.81
Overall	1192.26	38.92	1221.79	73.52	1265.29	51.61
SN						
Left	1303.52	43.87	1338.69	55.87	1337.68	48.30
Right	1326.41	40.16	1353.00	68.91	1355.96	48.97
Overall	1314.97	43.27	1345.84	61.98	1346.82	48.12
PAG	1750.91	74.30	1907.00	84.29	1952.60	47.68

STR striatum, *GPe* globus pallidus externa, *GPi* globus pallidus interna, *RN* red nucleus, *STN* subthalamic nucleus, *SN* substantia nigra, *PAG* periaqueductal grey

in standard MNI-space (STR: $r = 0.29$, t(106) = 3.05, $p = 0.021$; GPe: $r = 0.47$, t(106) = 5.35, $p < 0.001$; STN: $r = 0.28$, t(106) = 2.91, $p = 0.031$; RN: $r = 0.28$, t(106) = 2.90, $p = 0.032$; PAG: $r = 0.28$, t(106) = 2.94, $p = 0.028$) indicating the need for the visualization of the individual anatomy in aging populations (Keuken et al. 2013).

Effects of aging on T_1 values

All grey matter nuclei showed a positive correlation between the T_1 values and age (STR: $r = 0.32$, t(106) = 3.41, $p = 0.006$; GPe: $r = 0.44$, t(106) = 4.97, $p < 0.001$; GPi: $r = 0.47$, t(106) = 5.43, $p < 0.001$; STN: $r = 0.50$, t(106) = 5.78, $p < 0.001$; RN: $r = 0.60$, t(106) = 7.57, $p < 0.001$; SN: $r = 0.33$, t(106) = 3.53, $p = 0.004$; PAG: $r = 0.77$, t(53) = 8.54, $p < 0.001$). The non-thresholded T_1 values of the STR and PAG also showed a positive correlation with age (STR: $r = 0.26$, t(106) = 2.73, $p = 0.015$; PAG: $r = 0.77$, t(53) = 8.54, $p < 0.001$). An increase in T_1 values

is thought to reflect a decrease of myelinisation (Callaghan et al. 2014). See Fig. 2b for the T_1 values per structure; Table 2 and Fig. 3b for the average values per age group.

Effects of aging on T_2^* values

The STR and RN showed a negative correlation between the T_2^* values and age (STR: $r = -0.71$, t(106) = −10.15, $p < 0.001$; RN: $r = -0.49$, t(106) = −5.74, $p < 0.001$). Contrary to these structures, there was a positive correlation between the T_2^* values and age for the GPi and SN, two of which were found to have an increased volume with age (GPi: $r = 0.46$, t(106) = 5.28, $p < 0.001$; SN: $r = 0.34$, t(106) = 3.65, $p < 0.001$). The STN, GPe, and PAG did not show a significant correlation between age and T_2^* values. The T_2^* values for the non-thresholded STR indicated a negative correlation with age, whereas the PAG still did not show a significant correlation (STR: $r = -0.55$, t(106) = −6.62, $p < 0.001$). A change in T_2^* values is thought to reflect a change in ratio of the

Table 3 The mean and standard deviation of the T_2^* values in ms per structure and age group

Structure	Young		Middle-aged		Elderly	
	Mean	SD	Mean	SD	Mean	SD
STR						
Left	27.97	1.98	23.42	1.64	23.38	2.70
Right	28.00	1.89	23.23	1.63	22.02	2.52
Overall	27.97	1.92	23.33	1.61	22.70	2.63
GPe						
Left	12.95	1.20	13.56	2.62	20.07	15.89
Right	12.59	0.83	13.15	2.32	16.39	5.15
Overall	12.77	1.04	13.36	2.43	18.22	11.62
GPi						
Left	12.82	0.85	13.34	2.21	20.95	9.41
Right	12.65	0.92	13.07	1.57	22.26	10.86
Overall	12.74	0.88	13.20	1.88	21.61	9.88
RN						
Left	17.38	1.67	14.26	1.61	14.29	1.65
Right	17.14	1.30	14.69	1.83	14.00	1.90
Overall	17.26	1.49	14.48	1.70	14.15	1.73
STN						
Left	15.11	1.60	13.39	2.46	14.41	2.78
Right	14.98	1.45	13.61	2.11	14.41	2.85
Overall	15.05	1.51	13.50	2.25	14.41	2.73
SN						
Left	13.32	1.11	14.23	2.36	20.55	10.19
Right	13.12	0.94	16.00	8.20	19.37	9.22
Overall	13.22	1.03	15.12	5.99	19.96	9.44
PAG	42.31	2.84	40.85	3.50	43.92	5.73

STR striatum, *GPe* globus pallidus externa, *GPi* globus pallidus interna, *RN* red nucleus, *STN* subthalamic nucleus, *SN* substantia nigra, *PAG* periaqueductal grey

contribution of myelin or iron to the measured signal (Deistung et al. 2013; Stüber et al. 2014). See Fig. 2c for the T_2^* values per structure; Table 3 and Fig. 3c for the average values per age group.

Effects of aging on the QSM values

The STR, RN, and SN showed a positive correlation of age with the QSM values indicating an increase of iron concentration (STR: $r = 0.43$, t(106) = 4.80, $p < 0.001$; RN: $r = 0.45$, t(106) = 5.12, $p < 0.001$; SN: $r = 0.37$, t(106) = 3.974, $p = 0.001$). There was no statistically significant relationship between the QSM values and age for the GPe, GPi, STN or PAG. See Fig. 2d for the QSM values per structure; Table 4 and Fig. 3d for the average values per age group. See Fig. 4 for the spatial distribution of mean T_1, T_2^*, and QSM values within the striatum and globus pallidum per age group.

Relationship between qMRI values

To test whether the T_1, T_2^*, and QSM values are highly dependent on each other, the different modalities were correlated. For the RN only, the T_1 values correlated with the T_2^* ($r = -0.31$, t(104) = -3.30, $p = 0.009$) and QSM values ($r = 0.32$, t(104) = 3.48, $p = 0.005$). For the STR and RN there was a negative correlation between the QSM and T_2^* values (STR: $r = -0.57$, t(104) = -7.04, $p < 0.001$; RN: $r = -0.70$, t(104) = -10.05, $p < 0.001$), but for the SN, this correlation was positive ($r = 0.27$, t(104) = 2.91, $p = 0.031$). See Fig. 5 for the significant correlations between qMRI values per structure.

Probability maps

Using the linearly registered probability atlases, the maximum and mean percentage overlaps were calculated following (Diedrichsen et al. 2009). Except for the STN, the maximum percentage overlap was generally high

Table 4 The mean and standard deviation of the QSM concentration in ppm per structure and age group

Structure	Young		Middle-aged		Elderly	
	Mean	SD	Mean	SD	Mean	SD
STR						
Left	0.003	0.027	0.026	0.014	0.035	0.019
Right	0.010	0.029	0.025	0.011	0.035	0.019
Overall	0.007	0.028	0.025	0.012	0.035	0.019
GPe						
Left	0.111	0.038	0.120	0.015	0.130	0.044
Right	0.119	0.040	0.120	0.011	0.133	0.039
Overall	0.115	0.039	0.120	0.013	0.131	0.040
GPi						
Left	0.100	0.038	0.100	0.020	0.110	0.066
Right	0.111	0.043	0.111	0.021	0.116	0.052
Overall	0.106	0.041	0.106	0.021	0.113	0.058
RN						
Left	0.025	0.036	0.074	0.027	0.083	0.014
Right	0.031	0.036	0.074	0.025	0.084	0.020
Overall	0.028	0.036	0.074	0.026	0.083	0.017
STN						
Left	0.026	0.041	0.027	0.047	0.042	0.042
Right	0.029	0.046	0.034	0.025	0.029	0.029
Overall	0.027	0.043	0.030	0.037	0.036	0.036
SN						
Left	0.092	0.031	0.115	0.030	0.124	0.033
Right	0.098	0.036	0.117	0.024	0.141	0.046
Overall	0.095	0.034	0.115	0.026	0.133	0.040
PAG	−0.045	0.030	−0.057	0.017	−0.053	0.015

STR striatum, *GPe* globus pallidus externa, *GPi* globus pallidus interna, *RN* red nucleus, *STN* subthalamic nucleus, *SN* substantia nigra, *PAG* periaqueductal grey

across structures and age groups. Similarly, the mean percentage overlap was lowest for the STN compared to the other included structures. This might indicate either larger anatomical or increased registration variability for the STN compared to the other structures. As neighbouring structures of similar size and shape (RN, SN) did not show this trend, anatomical variability seems more plausible. This would need further testing with larger samples and more elaborate shape analysis to fully answer this question. See Table 5 for the maximum and mean overlap per structure and age group. Given that different registration procedures can result in differences in overlap, one would ideally only use the current probability atlases after using similar normalisation protocols (Diedrichsen et al. 2009; Klein et al. 2009). See Fig. 6 for the linearly registered probability atlases per structure and age group.

Discussion

Using ultra-high field 7T MRI, we show that healthy aging has variable anatomical effects on a number of subcortical structures. In line with previous reports we show that ventricular volume generally increased with age, and that the volume of most subcortical grey matter areas decrease (Barron et al. 1976; Scahill et al. 2003; Terribilli et al. 2011). In addition to volumetric changes the spatial location of several structures was also affected by age. For the STR, GPe, RN, STN, and PAG it was shown that the CoM in MNI space changed with age. This shift in location with age has been previously reported for the STN, using a range of different registration pipelines, but not, to the best of our knowledge, for the STR, GPe, RN, or PAG (Dunnen and Staal 2005; Kitajima et al. 2008; Keuken et al. 2013; Mavridis et al. 2014). These volumetric and positional changes should be taken into account in surgical procedures such as deep brain stimulation (DBS). For instance, one of the frequently targeted DBS structures for

Fig. 4 The spatial distribution of the mean T_1, T_2^*, and QSM values within the striatum and globus pallidum per age group at MNI Z coordinate 0. The linearly registered probability atlas was thresholded at 33% overlap
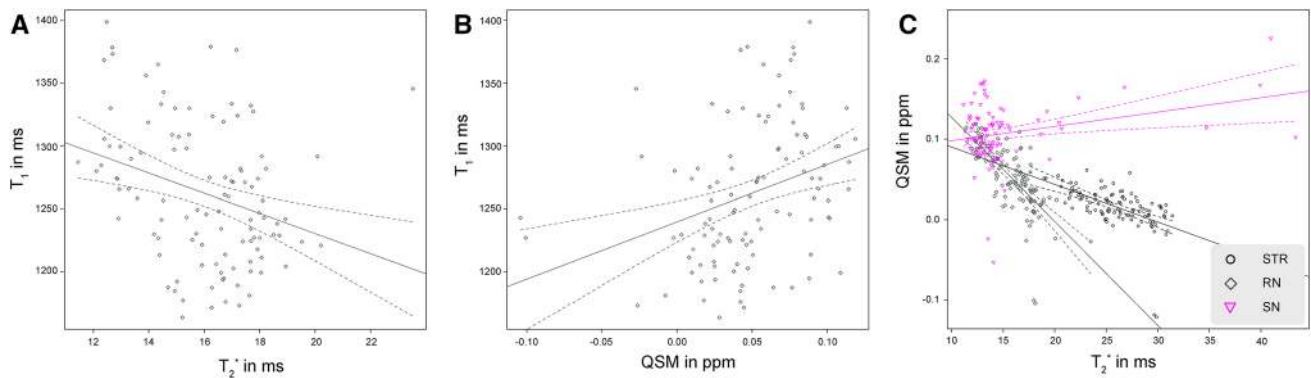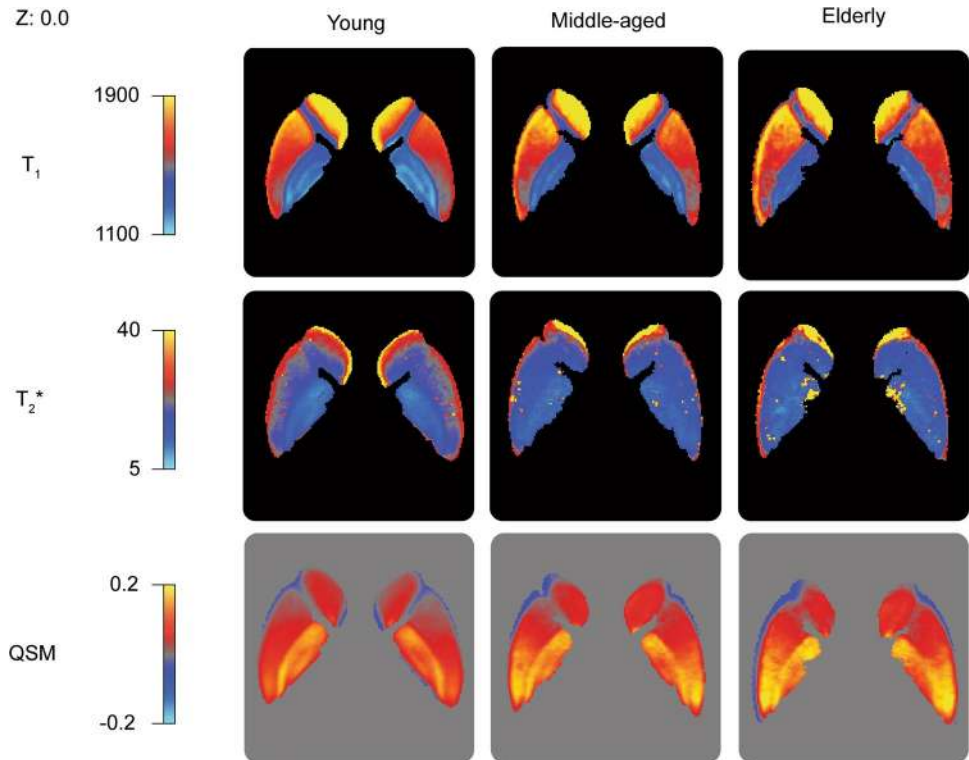

Fig. 5 The relationship between qMRI parameters. **a** The T_1 values versus the T_2^* values in the striatum. **b** The T_1 values versus the QSM values in the striatum. **c** The QSM values versus the T_2^* values in the striatum, red nucleus and substantia nigra. The regression lines indicate a significant correlation between qMRI parameters for a given structure. The dotted lines indicate 95% confidence interval. *STR* striatum, *RN* red nucleus, *RN* substantia nigra, *QSM* quantitative susceptibility mapping

Parkinson's disease is the STN (Deep-Brain Stimulation for Parkinson's Disease Study Group 2001; Follett and Torres-Russotto 2011; Schuepbach et al. 2013). There are several different strategies to determine the location of the stimulation site within the STN, but a prominent procedure is the indirect targeting of the STN using landmarks such as the AC-PC mid commissural point or the RN (Bejjani et al. 2000; Andrade-Souza et al. 2005; Fytagoridis and Blomstedt 2010). Given the changes in volume and location of the RN and STN, one might argue against this procedure of indirect targeting and instead use direct visualization of the STN, ideally with the use of ultra-high field MRI (Cho et al. 2010, 2011; Abosch et al. 2010; Beisteiner et al. 2011). In general, as indicated by the probability atlas, there is a large anatomical variability across the different age groups and structures. These volumetric and positional changes should be taken into account in surgical procedures such as deep brain stimulation (DBS).

In terms of quantitative MRI parameters, we show that for all included subcortical grey matter nuclei, the T_1

Table 5 The maximum and mean percentage overlap per linearly registered structure and age group

Structure	Young		Middle-aged		Elderly	
	Maximum	Mean	Maximum	Mean	Maximum	Mean
STR						
Left	100.00	42.94	100.00	47.01	100.00	46.82
Right	100.00	42.66	100.00	43.80	100.00	45.47
GPe						
Left	100.00	26.79	100.00	30.88	100.00	35.41
Right	100.00	26.26	100.00	30.10	100.00	35.22
GPi						
Left	100.00	22.09	99.14	26.52	100.00	23.89
Right	99.18	21.82	100.00	25.44	100.00	23.95
RN						
Left	100.00	25.14	100.00	30.87	100.00	28.72
Right	100.00	25.22	100.00	28.37	95.90	28.00
STN						
Left	65.09	9.11	49.27	8.53	61.14	14.24
Right	63.31	9.96	54.38	8.79	53.52	10.81
SN						
Left	90.42	18.10	98.22	22.93	99.40	25.84
Right	78.02	16.70	89.57	20.89	88.89	22.59
PAG	95.31	19.91	99.83	24.48	93.34	21.62

STR striatum, *GPe* globus pallidus externa, *GPi* globus pallidus interna, *RN* red nucleus, *STN* subthalamic nucleus, *SN* substantia nigra, *PAG* periaqueductal grey
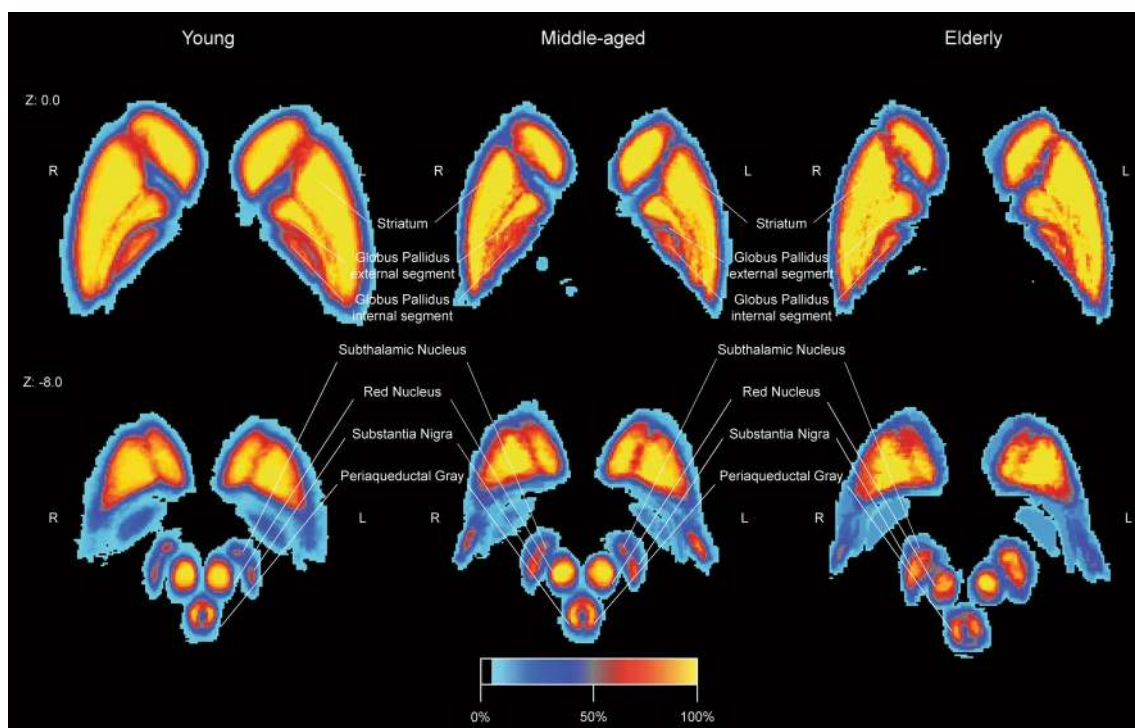
Fig. 6 The linearly registered probability atlas in MNI-space per age group. The colour intensity reflects the percentage overlap across the participants per age group. A 100% overlap for the young indicates that 30 participants shared that voxel, whereas a 100% overlap for the elderly indicates that nine participants shared that voxel

value gradually increased with age, possibly indicating a loss of myelin or incomplete remyelination (Zivadinov 2007; Stüber et al. 2014; Callaghan et al. 2014; Steiger et al. 2016). The T_2^* and QSM results were more variable and are thought to reflect different aspects of the iron and myelin content in the tissue (Deistung et al. 2013; Stüber et al. 2014). For instance, a decrease in myelin is thought to be indicated with a lengthening of T_2^* and an increase of QSM values, whereas an increase of iron is considered to shorten T_2^* and increase quantitative magnetic susceptibility (Deistung et al. 2013). QSM is thought to mainly reflect ferritin-bound iron in grey matter, with an increase in QSM indicating an increased iron concentration (Langkammer et al. 2012; Zheng et al. 2013; Stüber et al. 2014; Ropele and Langkammer 2016).

There was converging evidence for a potential increase of iron concentration with age within the STR and RN, which showed decreased T_2^* and increased magnetic susceptibility. In addition, there was a negative correlation between the T_2^* and QSM values, hinting at an increase of iron. This is in line with a recent meta-analysis indicating an aging effect on the accumulation of iron in the STR and RN (Daugherty and Raz 2013). No statistical significant effect of T_2^* or QSM were found for the GPe, STN, or PAG. The lack of results for the GPe where not surprising as the reported effect size of age on T_2^* values in the GP are relatively small and might be difficult to find with the current sample size (Daugherty and Raz 2013). The absence of a significant QSM correlation for the GP and no T_2^* changes in the PAG were reported previously (Lambert et al. 2013; Acosta-Cabronero et al. 2016). It was surprising to find no significant relationship between the T_2^* values in the STN and age. This contrasts with previous findings by our group using similar segmentation protocols and more recently by whole brain approaches (Keuken et al. 2013; Betts et al. 2016). As all three studies are based on cross-sectional designs with relative small sample sizes, there is a clear need for large sample longitudinal studies to answer the question whether age influences the T_2^* values in the STN.

The results for the GPi and SN are more challenging to interpret. For the SN, the increased T_1 indicates a potential decrease in myelin content, and the increased magnetic susceptibility shows a potential increase of iron content. The increase in QSM values in the SN has been reported previously (Bilgic et al. 2012; Gong et al. 2015; Acosta-Cabronero et al. 2016). The decrease of myelin for the SN is further supported by the positive correlation between the T_2^* and QSM values. For the GPi, an increase of T_2^* was found but no significant age effects were detected for the QSM values. The increase in T_2^* is more difficult to explain and is in direct contrast to the meta-analysis of Daugherty and Raz (2013). The increase of T_2^* may arise from a more uniform distribution of iron within the tissue, or may provide

additional evidence for the decrease of myelin (Siemonsen et al. 2008; Deistung et al. 2013).

These changes with age in quantitative MRI values have several methodological implications. The change in T_1 may well affect the accuracy of a number of automatic parcellation tools, such as FIRST or Freesurfer, which have been used to investigate volumetric changes in the subcortex with aging (e.g., Goodro et al. 2012; Liem et al. 2015). These parcellation tools are solely based on the contrast of a T_1-weighted image (Visser et al. 2016a) and could thus easily be influence by changes in the value of T_1 (Jernigan et al. 2001). Previous work by Wenger et al. (2014) and Lorio et al. (2014, 2016b) have indeed shown an age-related bias in automatic segmentation and that certain sequences are less prone to this age effect (Helms et al. 2009).

The change of T_2^* values might affect the sensitivity in fMRI studies. Since the optimal TE in a gradient-echo EPI sequence is equal to the T_2^* relaxation time, an effect of aging on the T_2^* values results in a change of BOLD sensitivity (Ugurbil et al. 2007; Koopmans et al. 2011; Norris 2012). It might be the case that when fMRI data is acquired for two age groups with the same TE this might result in a significant apparent difference which might actually be driven by changes in anatomy but not necessarily in function (e.g., Mell 2009; Eppinger et al. 2013).

Limitations

As with any cross-sectional study there is always the risk for cohort effects. Particularly when a small sample is used, it is not trivial to attribute the observed effects to individual variability or to healthy aging. The number of healthy elderly subjects that underwent all the UHF-MRI scans was relatively low and might be the cause of relatively low correlation coefficients. While this is true, it should be noted that cross-sectional and longitudinal studies generally show similar effects of aging, while the effects are more pronounced in longitudinal studies (Scahill et al. 2003). Another limitation is that the structures were parcellated using only one MRI contrast, which for most structures was shown to change with age. Though unlikely, the changes in T_1, T_2^*, and QSM values could have resulted in a shift of the perceptual boundaries, influencing the volumetric results, while the underlying true anatomy remained stable. A potential solution for this is to use multiple contrasts simultaneously to inform the parcellation. Recent parcellation tools have indeed shown that the combination of multiple MRI contrasts in a Bayesian framework improve the segmentation of subcortical structures (Kim et al. 2014; Visser et al. 2016b, a; Lorio et al. 2016a).

The estimation of the qMRI values and the relationship with the underlying tissue composition is not trivial (Weiskopf et al. 2015; Ropele and Langkammer 2016). In the current study the T_1 values were estimated using a well-characterized and tested MP2RAGE sequence, but it is acknowledged that the resulting T_1 maps may contain a residual transmit field bias which would result in less precise measures (Lutti et al. 2014). Nonetheless, the reported T_1 values of the GP are similar to a recent 7T multi-site test–retest validation study indicating that the T_1 values estimated from the MP2RAGE are stable (Voelker et al. 2016). The T_2^* values were estimated by fitting a mono-exponential fit on a multi-echo T_2^*-weighted volume (Chavhan et al. 2009) but it is known that the T_2^* values are influenced by the choice of TE, number of TE's, and the actual function used to estimate the T_2^* values (Yin et al. 2010; Milford et al. 2015). Although different methods were used to estimate T_2^*, the current T_2^* values for the STR, GP, SN, and RN resulted in a similar rank ordering as previous 7T MRI work (Khabipova et al. 2015). The same holds for the calculation of QSM values. These values are influenced by a number of variables during both the acquisition phase and the post-processing phase (Haacke et al. 2015; Ropele and Langkammer 2016).

While ultra-high field MRI has several benefits for imaging small subcortical structures it is not without methodological challenges (van der Zwaag et al. 2015). As the field strength increases, the B_0 inhomogeneity increases as well resulting in an inhomogeneous tissue contrast (van de Moortele et al. 2005; van der Zwaag et al. 2015). However, the autoshim facility of the 7T MRI scanner used is normally observed to provide a satisfactory shim, and is comparable to other 7T MRI sites (Voelker et al. 2016).

A final limitation is the low number of parcellated subcortical structures, given the total number of structures that are known to exist (Alkemade et al. 2013). We included only a small number of structures for several limiting reasons. The first one is the required time for careful manual delineation of each individual structure. The second, but more important, reason is that we selected only those structures that were easily visible with the contrast and spatial resolution employed. To discriminate more structures such as the thalamic nuclei, it may help to use specific MRI sequences that are tailored to that structure (Tourdias et al. 2014), improve the spatial resolution, or consider *post mortem* studies (Keren et al. 2015; Forstmann et al. in press). By reducing the voxel size, the partial volume effects (PVE) become less prominent. As the voxel resolution improves, the correction for subject motion becomes increasingly important and needs to be taken into account during the data acquisition (Tisdall et al. 2016). Prospective motion correction would additionally reduce the PVE and result in a higher SNR while allowing for higher spatial resolution (e.g., Stucht et al. 2015; Federau and Gallichan 2016). The need for reducing the PVE is crucial for smaller structures as their surface-area-to-volume ratio is larger (Vos et al. 2011).

Conclusion

Using quantitative ultra-high field 7T MRI, we were able to show variable age-related changes in anatomical features in several subcortical nuclei, as well as age-related changes in underlying MRI parameters that drive typical image contrast. These qMRI changes seem to be driven by different mechanisms: the increase of T_1 values indicate a global decrease of myelination across the subcortical structures, whereas some of the structures, T_2^* and QSM results indicate an iron accumulation with age.

Compliance with ethical standards

Ethical approval All procedures performed in studies involving human participants were in accordance with the ethical standards of the institutional and/or national research committee and with the 1964 Helsinki declaration and its later amendments or comparable ethical standards.

References

Abosch A, Yacoub E, Ugurbil K, Harel N (2010) An assessment of current brain targets for deep brain stimulation surgery with susceptibility-weighted imaging at 7 T. Neurosurgery 67:1745–1756. doi:10.1227/NEU.0b013e3181f74105

Acosta-Cabronero J, Betts MJ, Cardenas-Blanco A et al (2016) In vivo MRI mapping of brain iron deposition across the adult lifespan. 36:364–374. doi:10.1523/JNEUROSCI.1907-15.2016

Alkemade A, Keuken MC, Forstmann BU (2013) A perspective on terra incognita: uncovering the neuroanatomy of the human subcortex. Front Neuroanat. doi:10.3389/fnana.2013.00040

Andersson J, Jenkinson M, Smith S (2007) Non-linear registration, aka spatial normalisation. Technical Report TR07JA2, Oxford Centre for Functional Magnetic Resonance Imaging of the Brain, Department of Clinical Neurology, Oxford University,

Oxford, UK. Available at http://www.fmrib.ox.ac.uk/analysis/techrep

Andrade-Souza YM, Schwalb JM, Hamani C et al (2005) Comparison of three methods of targeting the subthalamic nucleus for chronic stimulation in Parkinson's disease. Neurosurgery 56:360–368. doi:10.1227/01.NEU.0000156547.24603.EE

Aquino D, Bizzi A, Grisoli M et al (2009) Age-related Iron deposition in the basal ganglia: quantitative analysis in healthy subjects. Radiology 252:165–172. doi:10.1148/radiol.2522081399

Barron SA, Jacobs L, Kinkel WR (1976) Changes in size of normal lateral ventricles during aging determined by computerized tomography. Neurology 26:1011–1011

Bastin ME, Clayden JD, Pattie A et al (2009) Diffusion tensor and magnetization transfer MRI measurements of periventricular white matter hyperintensities in old age. Neurobiol Aging 30:125–136. doi:10.1016/j.neurobiolaging.2007.05.013

Bazin P-L, Weiss M, Dinse J et al (2013) A computational framework for ultra-high resolution cortical segmentation at 7 T. NeuroImage 1–9. doi:10.1016/j.neuroimage.2013.03.077

Beisteiner R, Robinson S, Wurnig M et al (2011) Clinical fMRI: evidence for a 7 T benefit over 3 T. NeuroImage 57:1015–1021. doi:10.1016/j.neuroimage.2011.05.010

Bejjani BP, Dormont D, Pidoux B, Yelnik J, Damier P, Arnulf I, Bonnet AM, Marsault C, Agid Y, Philippon J, Cornu P (2000) Bilateral subthalamic stimulation for Parkinson's disease by using three-dimensional stereotactic magnetic resonance imaging and electrophysiological guidance. J Neurosurg 92(4):615–625

Benedetti B, Charil A, Rovaris M et al (2006) Influence of aging on brain gray and white matter changes assessed by conventional, MT, and DT MRI. Neurology 66:535–539

Betts MJ, Acosta-Cabronero J, Cardenas-Blanco A et al (2016) High-resolution characterisation of the aging brain using simultaneous quantitative susceptibility mapping (QSM) and R2* measurements at 7 T. NeuroImage 138:43–63. doi:10.1016/j.neuroimage.2016.05.024

Bilgic B, Pfefferbaum A, Rohlfing T et al (2012) MRI estimates of brain iron concentration in normal aging using quantitative susceptibility mapping. NeuroImage 59:2625–2635. doi:10.1016/j.neuroimage.2011.08.077

Callaghan MF, Freund P, Draganski B et al (2014) Widespread age-related differences in the human brain microstructure revealed by quantitative magnetic resonance imaging. Neurobiol Aging NBA 35:1862–1872. doi:10.1016/j.neurobiolaging.2014.02.008

Chavhan GB, Babyn PS, Thomas B et al (2009) Principles, techniques, and applications of T_2^*-based MR imaging and its special applications1. RadioGraphics 29:1433–1449. doi:10.1148/rg.295095034

Cherubini A, Péran P, Caltagirone C et al (2009) Aging of subcortical nuclei: microstructural, mineralization and atrophy modifications measured in vivo using MRI. NeuroImage 48:29–36. doi:10.1016/j.neuroimage.2009.06.035

Cho ZH, Kim YB, Han JY et al (2008) New brain atlas—mapping the human brain in vivo with 7.0 T MRI and comparison with postmortem histology: Will these images change modern medicine? Int J Imaging Syst Technol 18:2–8

Cho ZH, Min HK, Oh SH et al (2010) Direct visualization of deep brain stimulation targets in Parkinson disease with the use of 7-tesla magnetic resonance imaging. J Neurosurg 113:1–9

Cho ZH, Kim JM, Park SY et al (2011) Direct visualization of Parkinson's disease by in vivo human brain imaging using 7.0 T magnetic resonance imaging. Mov Disord 26:713–718. doi:10.1002/mds.23465

Cohen-Adad J, Polimeni JR, Helmer KG et al (2012) T_2^* mapping and B0 orientation-dependence at 7 T reveal cyto- and myeloarchitecture organization of the human cortex. NeuroImage 60:1006–1014. doi:10.1016/j.neuroimage.2012.01.053

Courchesne E, Chisum HJ, Townsend J et al (2000) Normal brain development and aging: quantitative analysis at in vivo MR imaging in healthy volunteers. Radiology 216:672–682

Daugherty A, Raz N (2013) Age-related differences in iron content of subcortical nuclei observed in vivo: a meta-analysis. NeuroImage 70:113–121. doi:10.1016/j.neuroimage.2012.12.040

Deistung A, Schäfer A, Schweser F et al (2013) Toward in vivo histology: a comparison of quantitative susceptibility mapping (QSM) with magnitude-, phase-, and R2*-imaging at ultra-high magnetic field strength. NeuroImage 65:299–314. doi:10.1016/j.neuroimage.2012.09.055

Dice LR (1945) Measures of the amount of ecologic association between species. Ecology 26:297–302

Diedrichsen J, Balsters JH, Flavell J et al (2009) A probabilistic MR atlas of the human cerebellum. NeuroImage 46:39–46. doi:10.1016/j.neuroimage.2009.01.045

Dinse J, Härtwich N, Waehnert MD, et al (2015) A cytoarchitecture-driven myelin model reveals area-specific signatures in human primary and secondary areas using ultra-high resolution in-vivo brain MRI. NeuroImage 114:71–87. doi:10.1016/j.neuroimage.2015.04.023

Deep-Brain Stimulation for Parkinson's Disease Study Group (2001) Deep-brain stimulation of the subthalamic nucleus or the pars interna of the globus pallidus in Parkinson's disease. N Engl J Med 345(13):956–963

Draganski B, Ashburner J, Hutton C et al (2011) Regional specificity of MRI contrast parameter changes in normal ageing revealed by voxel-based quantification (VBQ). NeuroImage 55:1423–1434. doi:10.1016/j.neuroimage.2011.01.052

Dunnen Den WF, Staal MJ (2005) Anatomical alterations of the subthalamic nucleus in relation to age: a postmortem study. Mov Disord 20:893–898. doi:10.1002/mds.20417

Eppinger B, Schuck NW, Nystrom LE, Cohen JD (2013) Reduced striatal responses to reward prediction errors in older compared with younger adults. J Neurosci 33:9905–9912. doi:10.1523/JNEUROSCI.2942-12.2013

Federau C, Gallichan D (2016) Motion-correction enabled ultra-high resolution In-vivo 7 T-MRI of the brain. PloS One 11:e0154974–e0154912. doi:10.1371/journal.pone.0154974

Fjell AM, Walhovd KB (2010) Structural brain changes in aging: courses, causes and cognitive consequences. Rev Neurosci 21:187–221

Follett KA, Torres-Russotto D (2011) Deep brain stimulation of globus pallidus interna, subthalamic nucleus, and pedunculopontine nucleus for Parkinson's disease: Which target? Parkinsonism Realt Disord 18:S165–S167. doi:10.1016/S1353-8020(11)70051-7

Forstmann BU, Keuken MC, Schäfer A et al (2014) Multi-modal ultra-high resolution structural 7-Tesla MRI data repository. Scient Data 1:140050–140058. doi:10.1038/sdata.2014.50

Forstmann BU, de Hollander G, van Maanen L et al (in press). Towards a mechanistic understanding of the human subcortex. Nat Rev Neurosci

Fukunaga M, Li TQ, van Gelderen P et al (2010) Layer-specific variation of iron content in cerebral cortex as a source of MRI contrast. Proc Nat Acad Sci 107:3834–3839. doi:10.1073/pnas.0911177107

Fytagoridis A, Blomstedt P (2010) Complications and side effects of deep brain stimulation in the posterior subthalamic area. Stereotact Funct Neurosurg 88:88–93. doi:10.1159/000271824

Ge Y, Grossman RI, Babb JS, Rabin ML, Mannon LJ, Kolson DL (2002) Age-related total gray matter and white matter changes in normal adult brain. Part I: volumetric MR imaging analysis. Am J Neuroradiol 23(8):1327–1333

Gong N-J, Wong C-S, Hui ES et al (2015) Hemisphere, gender and age-related effects on iron deposition in deep gray

matter revealed by quantitative susceptibility mapping. NMR Biomed 28:1267–1274. doi:10.1002/nbm.3366

Good CD, Johnsrude IS, Ashburner J et al (2001) A voxel-based morphometric study of ageing in 465 normal adult human brains. NeuroImage 14:21–36. doi:10.1006/nimg.2001.0786

Goodro M, Sameti M, Patenaude B, Fein G (2012) Age effect on subcortical structures in healthy adults. Psychiatr Res Neuroimaging 203:38–45. doi:10.1016/j.pscychresns.2011.09.014

Greenberg DL, Messer DF, Payne ME et al (2008) Aging, gender, and the elderly adult brain: an examination of analytical strategies. Neurobiol Aging 29:290–302. doi:10.1016/j.neurobiolaging.2006.09.016

Haacke EM, Liu S, Buch S et al (2015) Quantitative susceptibility mapping: current status and future directions. Magn Reson Imaging 33:1–25. doi:10.1016/j.mri.2014.09.004

Haase A, Frahm J, Matthaei D et al (1986) FLASH imaging. Rapid NMR imaging using low flip-angle pulses. J Magn Reson 67:258–266

Haber SN, Gdowski MJ (2004) The basal ganglia. In: Paxinos G, Mai JK (ed) The human nervous system, 2nd edn. Academic Press, London, p 676–738

Haber SN, Knutson B (2009) The reward circuit: linking primate anatomy and human imaging. Neuropsychopharmacology 35:4–26. doi:10.1038/npp.2009.129

Hallgren B, Sourander P (1958) The effect of age on the non-haemin iron in the human brain. J Neurochem 3:41–51

Helms G, Draganski B, Frackowiak R et al (2009) Improved segmentation of deep brain grey matter structures using magnetization transfer (MT) parameter maps. NeuroImage 47:194–198. doi:10.1016/j.neuroimage.2009.03.053

Jenkinson M, Smith S (2001) A global optimisation method for robust affine registration of brain images. Med Image Anal 5:143–156

Jenkinson M, Bannister P, Brady M, Smith S (2002) Improved optimization for the robust and accurate linear registration and motion correction of brain images. NeuroImage 17:825–841. doi:10.1006/nimg.2002.1132

Jenkinson M, Beckmann CF, Behrens TEJ et al (2012) FSL. NeuroImage 62:782–790. doi:10.1016/j.neuroimage.2011.09.015

Jernigan TL, Archibald SL, Fennema-Notestine C (2001) Effects of age on tissues and regions of the cerebrum and cerebellum. Neurobiol Aging 22:581–594. doi:10.1016/s0197-4580(01)00217-2

Keren NI, Taheri S, Vazey EM et al (2015) Histologic validation of locus coeruleus MRI contrast in post-mortem tissue. NeuroImage 1–11. doi:10.1016/j.neuroimage.2015.03.020

Keuken MC, Bazin PL, Schafer A et al (2013) Ultra-high 7 T MRI of structural age-related changes of the subthalamic. Nucleus 33:4896–4900. doi:10.1523/JNEUROSCI.3241-12.2013

Keuken MC, Bazin PL, Crown L et al (2014) Quantifying inter-individual anatomical variability in the subcortex using 7 T structural MRI. NeuroImage 94:40–46. doi:10.1016/j.neuroimage.2014.03.032

Khabipova D, Wiaux Y, Gruetter R, Marques JP (2015) A modulated closed form solution for quantitative susceptibility mapping — A thorough evaluation and comparison to iterative methods based on edge prior knowledge. NeuroImage 107:163–174. doi:10.1016/j.neuroimage.2014.11.038

Kim J, Lenglet C, Duchin Y et al (2014) Semiautomatic segmentation of brain subcortical structures from high-field MRI. IEEE J Biomed Health Inform 18:1678–1695. doi:10.1109/JBHI.2013.2292858

Kitajima M, Korogi Y, Kakeda S et al (2008) Human subthalamic nucleus: evaluation with high-resolution MR imaging at 3.0 T. Neuroradiology 50:675–681. doi:10.1007/s00234-008-0388-4

Klein A, Andersson J, Ardekani BA et al (2009) Evaluation of 14 nonlinear deformation algorithms applied to human brain MRI registration. NeuroImage 46:786–802. doi:10.1016/j.neuroimage.2008.12.037

Koenig SH (1991) Cholesterol of myelin is the determinant of gray-white contrast in MRI of brain. Magn Reson Med 20:285–291. doi:10.1002/mrm.1910200210

Koopmans PJ, Barth M, Orzada S, Norris DG (2011) Multi-echo fMRI of the cortical laminae in humans at 7 T. NeuroImage 1–41. doi:10.1016/j.neuroimage.2011.02.042

Lambert C, Chowdhury R, Fitzgerald T et al (2013) Characterizing aging in the human brainstem using quantitative multimodal MRI analysis. Front Hum Neurosci. doi:10.3389/fnhum.2013.00462

Langkammer C, Schweser F, Krebs N et al (2012) Quantitative susceptibility mapping (QSM) as a means to measure brain iron? A post mortem validation study. NeuroImage 62:1593–1599. doi:10.1016/j.neuroimage.2012.05.049

Lebel C, Gee M, Camicioli R et al (2012) Diffusion tensor imaging of white matter tract evolution over the lifespan. NeuroImage 60:340–352. doi:10.1016/j.neuroimage.2011.11.094

Lee J, Shmueli K, Fukunaga M et al (2010) Sensitivity of MRI resonance frequency to the orientation of brain tissue microstructure. Proc Natl Acad Sci USA 107:5130–5135. doi:10.1073/pnas.0910222107

Lemaitre H, Goldman AL, Sambataro F et al (2012) Normal age-related brain morphometric changes: nonuniformity across cortical thickness, surface area and gray matter volume? NBA 33:617.e1–617.e9. doi:10.1016/j.neurobiolaging.2010.07.013

Lenglet C, Abosch A, Yacoub E et al (2012) Comprehensive in vivo mapping of the human basal ganglia and thalamic connectome in individuals using 7 T MRI. PloS One 7:e29153. doi:10.1371/journal.pone.0029153.t001

Li W, Wu B, Batrachenko A et al (2013) Differential developmental trajectories of magnetic susceptibility in human brain gray and white matter over the lifespan. Hum Brain Mapp 35:2698–2713. doi:10.1002/hbm.22360

Liem F, Mérillat S, Bezzola L et al (2015) Reliability and statistical power analysis of cortical and subcortical FreeSurfer metrics in a large sample of healthy elderly. NeuroImage 108:95–109. doi:10.1016/j.neuroimage.2014.12.035

Lorio S, Lutti A, Kherif F et al (2014) Disentangling in vivo the effects of iron content and atrophy on the ageing human brain. NeuroImage 103:280–289. doi:10.1016/j.neuroimage.2014.09.044

Lorio S, Fresard S, Adaszewski S et al (2016a) New tissue priors for improved automated classification of subcortical brain structures on MRI. NeuroImage 130:157–166. doi:10.1016/j.neuroimage.2016.01.062

Lorio S, Kherif F, Ruef A et al (2016b) Neurobiological origin of spurious brain morphological changes: a quantitative MRI study. Hum Brain Mapp n/a–n/a. doi:10.1002/hbm.23137

Lutti A, Dick F, Sereno MI, Weiskopf N (2014) Using high-resolution quantitative mapping of R1 as an index of cortical myelination. NeuroImage 1–13. doi:10.1016/j.neuroimage.2013.06.005

Maniega SM, Hernández MCV, Clayden JD et al (2015) White matter hyperintensities and normal-appearing white matter integrity in the aging brain. NBA 36:909–918. doi:10.1016/j.neurobiolaging.2014.07.048

Marques JP, Gruetter R (2013) New developments and applications of the MP2RAGE sequence - focusing the contrast and high spatial resolution R1 mapping. PloS One 8:e69294–e69211. doi:10.1371/journal.pone.0069294

Marques JP, Kober T, Krueger G et al (2010) MP2RAGE, a self bias-field corrected sequence for improved segmentation and T_1-mapping at high field. NeuroImage 49:1271–1281. doi:10.1016/j.neuroimage.2009.10.002

Mavridis I, Boviatsis E, Anagnostopoulou S (2014) Stereotactic anatomy of the human subthalamic nucleus: providing coordinates

for accurate electrode placement. J Neurol Surg A Cent Eur Neurosurg 75:289–298. doi:10.1055/s-0034-1368093

McRobbie DW, Moore EA, Graves MJ, Prince MR (2006) MRI from picture to proton, 1st edn. Cambridge University Press, Cambridge

Mell T (2009) Altered function of ventral striatum during reward-based decision making in old age. Front Hum Neurosci. doi:10.3389/neuro.09.034.2009

Milford D, Rosbach N, Bendszus M, Heiland S (2015) Mono-exponential fitting in T_2-relaxometry: relevance of offset and first echo. PloS One 10:e0145255–e0145213. doi:10.1371/journal.pone.0145255

Mortamet B, Zeng D, Gerig G, Prastawa M, Bullitt E (2005) Effects of healthy aging measured by intracranial compartment volumes using a designed MR brain database. Med Image Comput Comput Assist Interv 8(Pt 1):383–391

Mueller EA, Moore MM, Kerr D et al (1998) Brain volume preserved in healthy elderly through the eleventh decade. Neurology 51:1555–1562

Neto LL, Oliveira E, Correia F, Ferreira AG (2008) The human nucleus accumbens: where is it? a stereotactic, anatomical and magnetic resonance imaging study. Neuromodul Technol Neural Interface 11:13–22

Norris DG (2012) Spin-echo fMRI: the poor relation? NeuroImage 62:1109–1115. doi:10.1016/j.neuroimage.2012.01.003

Okubo G, Okada T, Yamamoto A et al (2015) MP2RAGE for deep gray matter measurement of the brain: a comparative study with MPRAGE. J Magn Reson Imaging 43:55–62. doi:10.1002/jmri.24960

Oldfield RC (1971) The assessment and analysis of handedness: the Edinburgh inventory. Neuropsychologia 9:97–113

Persson N, Wu J, Zhang Q et al (2015) Age and sex related differences in subcortical brain iron concentrations among healthy adults. NeuroImage 122:385–398. doi:10.1016/j.neuroimage.2015.07.050

Pfefferbaum A, Adalsteinsson E, Rohlfing T, Sullivan EV (2009) MRI estimates of brain iron concentration in normal aging: comparison of field-dependent (FDRI) and phase (SWI) methods. NeuroImage 47:493–500. doi:10.1016/j.neuroimage.2009.05.006

Raz N, Rodrigue KM (2006) Differential aging of the brain: patterns, cognitive correlates and modifiers. Neurosci Biobehav Rev 30:730–748. doi:10.1016/j.neubiorev.2006.07.001

Ropele S, Langkammer C (2016) Iron quantification with susceptibility. NMR Biomed 1–9. doi:10.1002/nbm.3534

Saito N, Sakai O, Ozonoff Al, Jara H (2009) Relaxo-volumetric multispectral quantitative magnetic resonance imaging of the brain over the human lifespan: global and regional aging patterns. Magn Reson Imaging 27:895–906. doi:10.1016/j.mri.2009.05.006

Salat DH, Kaye JA, Janowsky JS (2002) Greater orbital prefrontal volume selectively predicts worse working memory performance in older adults. Cereb Cortex 12:494–505. doi:10.1093/cercor/12.5.494

Salat DH, Buckner RL, Snyder AZ et al (2004) Thinning of the cerebral cortex in aging. Cereb Cortex 14:721–730

Scahill RI, Frost C, Jenkins R et al (2003) A longitudinal study of brain volume changes in normal aging using serial registered magnetic resonance imaging. Arch Neurol 60:989–994. doi:10.1001/archneur.60.7.989

Schäfer A, Wharton S, Gowland P, Bowtell R (2009) Using magnetic field simulation to study susceptibility-related phase contrast in gradient echo MRI. NeuroImage 48:126–137. doi:10.1016/j.neuroimage.2009.05.093

Schenker C, Meier D, Wichmann W et al (1993) Age distribution and iron dependency of the T_2 relaxation time in the globus pallidus and putamen. Neuroradiology 35:119–124

Schuepbach WMM, Rau J, Knudsen K et al (2013) Neurostimulation for Parkinson's disease with early motor complications. N Engl J Med 368:610–622. doi:10.1056/NEJMoa1205158

Schweser F, Deistung A, Lehr BW, Reichenbach JR (2011) Quantitative imaging of intrinsic magnetic tissue properties using MRI signal phase: an approach to in vivo brain iron metabolism? NeuroImage 54:2789–2807. doi:10.1016/j.neuroimage.2010.10.070

Schweser F, Deistung A, Sommer K, Reichenbach JR (2012) Toward online reconstruction of quantitative susceptibility maps: Superfast dipole inversion. Magn Reson Med 69:1581–1593. doi:10.1002/mrm.24405

Schweser F, Deistung A, Reichenbach JR (2016) Foundations of MRI phase imaging and processing for Quantitative Susceptibility Mapping (QSM). Zeitschrift für medizinische Physik 26:6–34. doi:10.1016/j.zemedi.2015.10.002

Siemonsen S, Finsterbusch J, Matschke J et al (2008) Age-dependent normal values of T_2^* and T_2' in brain parenchyma. AJNR Am J Neuroradiol 29:950–955. doi:10.3174/ajnr.A0951

Silver NC, Good CD, Barker GJ, MacManus DG (1997) Sensitivity of contrast enhanced MRI in multiple sclerosis. Effects of gadolinium dose, magnetization transfer contrast and delayed imaging. Brain 120:1149–1161. doi:10.1093/brain/120.7.1149

Smith SM (2002) Fast robust automated brain extraction. Hum Brain Mapp 17:143–155. doi:10.1002/hbm.10062

Steen RG, Gronemeyer SA, Taylor JS (1995) Age-related changes in proton T_1 values of normal human brain. J Magn Reson Imaging 5:43–48. doi:10.1002/jmri.1880050111

Steiger JH (1980) Tests for comparing elements of a correlation matrix. Psychol Bull 87:245–251. doi:10.1037/0033-2909.87.2.245

Steiger TK, Weiskopf N, Bunzeck N (2016) Iron level and myelin content in the ventral striatum predict memory performance in the aging brain. J Neurosci 36:3552–3558. doi:10.1523/JNEUROSCI.3617-15.2016

Stüber C, Morawski M, Schäfer A et al (2014) Myelin and iron concentration in the human brain: a quantitative study of MRI contrast. NeuroImage 93:95–106. doi:10.1016/j.neuroimage.2014.02.026

Stucht D, Danishad KA, Schulze P et al (2015) Highest resolution in vivo human brain MRI using prospective motion correction. PLoS One 10:e0133921. doi:10.1371/journal.pone.0133921.s003

Team RC (2013) R: a language and environment for statistical computing.

Terribilli DB, Schaufelberger MS, Duran FLS et al (2011) Age-related gray matter volume changes in the brain during non-elderly adulthood. NBA 32:354–368. doi:10.1016/j.neurobiolaging.2009.02.008

Tisdall MD, Reuter M, Qureshi A et al (2016) Prospective motion correction with volumetric navigators (vNavs) reduces the bias and variance in brain morphometry induced by subject motion. NeuroImage 127:11–22. doi:10.1016/j.neuroimage.2015.11.054

Tourdias T, Saranathan M, Levesque IR et al (2014) Visualization of intra-thalamic nuclei with optimized white-matter-nulled MPRAGE at 7 T. NeuroImage 84:534–545. doi:10.1016/j.neuroimage.2013.08.069

Ugurbil K, Adriany G, Akgun C et al (2007) High magnetic fields for imaging cerebral morphology, function, and biochemistry. In: Robitaille P-M, Berliner L (eds) Ultra high field magnetic resonance imaging. Springer, New York, p 285–342

van de Moortele P-F, Akgun C, Adriany G et al (2005) B1 destructive interferences and spatial phase patterns at 7 T with a head transceiver array coil. Magn Reson Med 54:1503–1518. doi:10.1002/mrm.20708

van der Zwaag W, Schäfer A, Marques JP et al (2015) Recent applications of UHF-MRI in the study of human brain function

and structure: a review. NMR Biomed n/a–n/a. doi:10.1002/nbm.3275

Visser E, Keuken MC, Douaud G et al (2016a) Automatic segmentation of the striatum and globus pallidus using MIST: multimodal image segmentation tool. NeuroImage 125:479–497. doi:10.1016/j.neuroimage.2015.10.013

Visser E, Keuken MC, Forstmann BU, Jenkinson M (2016b) Automated segmentation of the substantia nigra, subthalamic nucleus and red nucleus in 7 T data at young and old age. NeuroImage 139:324–336. doi:10.1016/j.neuroimage.2016.06.039

Voelker MN, Kraff O, Brenner D et al (2016) The traveling heads: multicenter brain imaging at 7 T. 1–17. doi:10.1007/s10334-016-0541-8

Voorn P, Vanderschuren LJMJ, Groenewegen HJ et al (2004) Putting a spin on the dorsal–ventral divide of the striatum. Trends Neurosci 27:468–474. doi:10.1016/j.tins.2004.06.006

Vos SB, Jones DK, Viergever MA et al (2011) Partial volume effect as a hidden covariate in DTI analyses. NeuroImage 55(4):1566–1576. doi:10.1016/j.neuroimage.2011.01.048

Walhovd KB, Fjell AM, Reinvang I et al (2005) Effects of age on volumes of cortex, white matter and subcortical structures. Neurobiol Aging 26:1261–1270. doi:10.1016/j.neurobiolaging.2005.05.020

Weiskopf N, Mohammadi S, Lutti A, Callaghan MF (2015) Advances in MRI-based computational neuroanatomy. Curr Opin Neurol 28:313–322. doi:10.1097/wco.0000000000000222

Wenger E, Mårtensson J, Noack H et al (2014) Comparing manual and automatic segmentation of hippocampal volumes: reliability and validity issues in younger and older brains. Hum Brain Mapp 35:4236–4248. doi:10.1002/hbm.22473

Whittall KP, Mackay AL, Graeb DA et al (1997) In vivo measurement of T_2 distributions and water contents in normal human brain. Magn Reson Med 37:34–43. doi:10.1002/mrm.1910370107

Yeatman JD, Wandell BA, Mezer AA (2014) Lifespan maturation and degeneration of human brain white matter. Nat Commun 5:1–12. doi:10.1038/ncomms5932

Yin X, Shah S, Katsaggelos AK (2010) Improved R2* measurement accuracy with absolute SNR truncation and optimal coil combination. NMR Biomed 23:1127–1136. doi:10.1002/nbm.1539

Zecca L, Youdim M, Riederer P et al (2004) Iron, brain ageing and neurodegenerative disorders. Nat Rev Neurosci 5:863–873

Zheng W, Nichol H, Liu S et al (2013) Measuring iron in the brain using quantitative susceptibility mapping and X-ray fluorescence imaging. NeuroImage 78:68–74. doi:10.1016/j.neuroimage.2013.04.022

Zivadinov R (2007) Can imaging techniques measure neuroprotection and remyelination in multiple sclerosis? Neurology 68:S72–S82. doi:10.1212/01.wnl.0000275236.51129.d2